

1. Vapour Sensing System for Transistor Biosensing

1.1. General Overview

Through the adaptation of an existing setup, a custom vapour delivery system was developed to measure the response of field-effect biosensors to vapour. To achieve this goal, the new system needed to meet three requirements:

- The ability to automatically deliver a vapour to an enclosed environment in a controlled manner.
- The ability to collect measurements from a sensor device within that environment.
- The ability to collect data from off-the-shelf reference sensors monitoring the same environment, for comparison with data collected by the novel biosensor.

The existing system had a limited ability to meet the first two requirements, but was not able to take reference measurements of vapour flow. To implement new elements that would enable the system to fulfill all three requirements, a two-step development approach was taken across the course of the thesis. The changes made with each step of the redesign are outlined in Section 1.3.

Three mass flow controllers (MFC) were used to precisely control and monitor the flow of nitrogen into the system in units of standard cubic centimeters per minute (sccm). The manner in which these controllers were configured in the system is discussed in Section 1.2.1. The reference sensors chosen were a photoionisation detector (Ametek Mocon) and relative humidity and temperature indicator (Telaire). The photoionisation detector is able to monitor a wide range of volatile organic compounds, but cannot monitor compounds with an ionisation energy exceeding 10.6 eV. This includes nitrogen, oxygen, carbon dioxide, argon and water [1], [2]. Therefore, the photoionisation detector (PID) should not respond to either ambient air or standard nitrogen flow through the detector. As we would also like to monitor the presence of water vapour in the system, we use a relative humidity indicator (RHI). The operation of these reference sensors is discussed further in Section 1.2.2.

1. Vapour Sensing System for Transistor Biosensing

1.2. Technical Notes

1.2.1. Delivery System

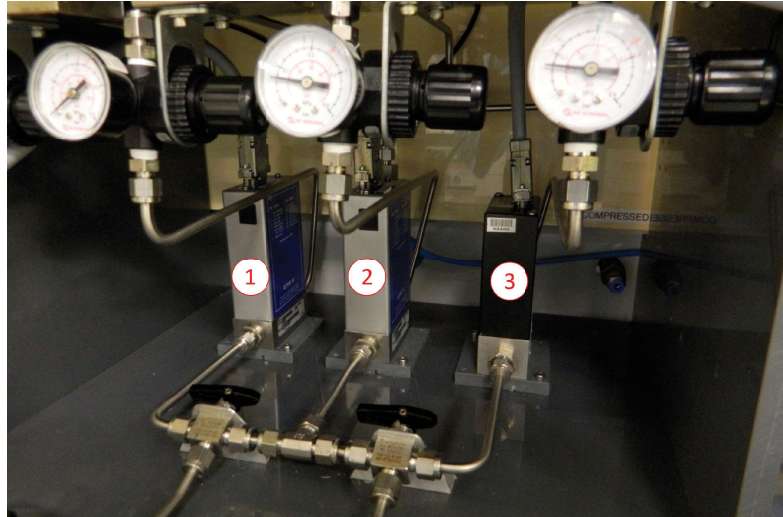


Figure 1.1.: Image of the three mass flow controllers (MFCs) of the Te Herenga Waka - Victoria University of Wellington cleanroom vapour delivery system, each with a regulator to set the pressure at the MFC inlet. (1) is the 20 sccm full-scale flow MFC, (2) is the 200 sccm full-scale flow MFC, and (3) is the 500 sccm full-scale flow MFC.

Three mass flow controller and their associated regulators sit in an covered enclosure, seen from the front in Figure 1.1. These are used to control the nitrogen flow rate through two different lines towards the chamber, the carrier line and dilution line. The lines merge at a mixing point about a metre before the device chamber, which contains the device being analysed. Each line consist of a mix of stainless steel and flexible PVC tubing, with various Swagelok fittings and valves. These valves include check valves, to ensure there is no backflow of vapour within the system. The carrier line connects flow to a 10 mL Schott bottle (Duran) containing analyte, shown in Figure 1.2. The vapour from the volatile analyte is then carried by nitrogen flow through the carrier line. A three-way valve determines whether the analyte vapour is then carried towards the mixing point or sent into the fumehood via the exhaust. The dilution line separately delivers flow to the mixing point, modifying the flow pushing the analyte vapour towards the chamber.

The setup is designed so that only one mass flow controller is directed through a single line at a time. The mass flow controller with a full-scale flow of 500 sccm (standard cubic centimeters per minute) can only be directed through the dilution line, and the mass flow controller with a full-scale flow of 20 sccm can only be directed through the carrier line. The mass flow controller with a full-scale flow of 200 sccm can be directed

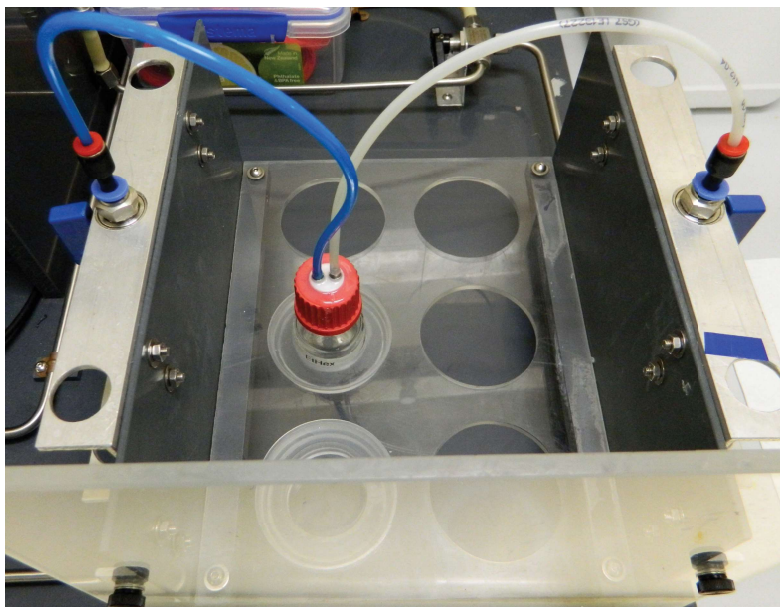


Figure 1.2.: Image of the analyte bottle, used to hold a volatile compound which provides vapour to the carrier line, either through bubbling or headspace sampling.

through the dilution line or carrier line. The electronic integration and programming of the mass flow controllers is described in Section 1.2.3.

1.2.2. Reference Sensors

Two reference sensors were added to the vapour delivery setup to compare the response to vapour by the fabricated sensor device with some reference signal. These reference sensors are a photoionisation detector (Ametek Mocon) and a relative humidity and temperature indicator (Telaire). The layout of these reference sensors (and their associated peripherals) relative to the device chamber is shown in Figure 1.3. These components are on a raised platform directly above the mass flow controller enclosure. Vapour flowing through the device chamber passes into a cylindrical manifold with three outlets. One outlet is the system exhaust, one flows into relative humidity indicator chamber, and one flows into the photoionisation detector. A dial-controlled micro diaphragm pump is used to set the flow rate from the manifold into the photoionisation detector, with a flowmeter used to monitor this flow rate.

The electronic integration and programming of the relative humidity and temperature indicator is described in Section 1.2.3. The photoionisation detector was connected to a laptop directly via USB, then controlled and monitored using the supplier-provided VOC-TRAQ II software package.

1. Vapour Sensing System for Transistor Biosensing

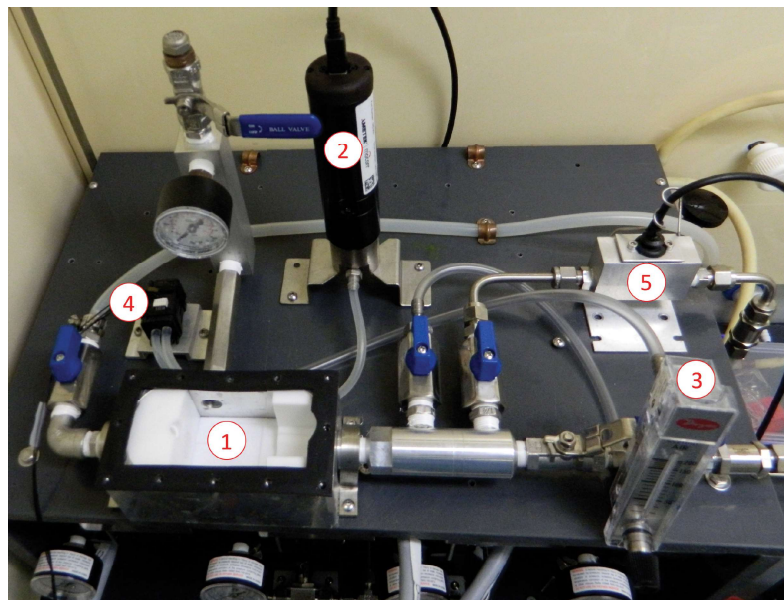


Figure 1.3.: Image of the device chamber, reference sensors and other related components. The components are labelled as follows: (1) Device chamber, (2) Photoionisation detector (PID), (3) Flowmeter from chamber to PID, (4) Micropump from chamber to PID, (5) Relative humidity and temperature monitor.

Relative Humidity and Temperature Indicator

The relative humidity and temperature indicator used here is a capacitive humidity sensor [3]. It consists of a capacitor with a hygroscopic polymer as the capacitor dielectric. As room temperature water has a much larger dielectric constant than the polymer dielectric, absorption of water by the polymer leads to increased sensor capacitance [4]. The sensor capacitance, corresponding to the amount of moisture absorbed by the polymer and therefore the relative humidity, is then translated by the sensor into a calibrated electronic output. This output is then processed using the hardware and software described in Section 1.2.3 to give a value for the relative humidity. The sensor has a quoted relative humidity (RH) accuracy of $\pm 2.0\%$ when RH is below 80%, and has a quoted temperature accuracy of 0.5°C [3].

The absolute humidity (AH), the mass of water vapour within a set volume, can be calculated in gm^{-3} using Equation 1.1, where $C = 2.16679 \text{ gKJ}^{-1}$, P_W is the water vapour pressure (in Pa) and T is the temperature (in K) [5].

$$AH = C \frac{P_W}{T} \quad (1.1)$$

For temperatures between -20°C and 50°C , water vapour pressure P_W (in hPa) can be approximated using Equation 1.2, where RH is relative humidity, T is temperature in $^\circ\text{C}$, A = 6.116441 hPa, m = 7.591386 and $T_n = 240.7263^\circ\text{C}$ [5].

$$P_W = RH \times A \times 10^{(mT/(T+T_n))} \quad (1.2)$$

Photoionisation Detector

A photoionisation detector (PID) can be used to continuously monitor volatile organic compounds by measuring the extent to which vapour molecules passing through the detector can be ionised. A small percentage of vapour molecules flowing into the detector diffuse into a sensor cavity. This cavity is bounded on each side by a pair of electrodes. A lamp in the body of the detector radiates UV light through a window into this cavity. The vapour molecules have their outer-most electrons excited and removed when struck with these high-energy photons. The ionised molecules then drift towards the sensor cathode, while free electrons drift towards the sensor anode. This results in a current proportional to the concentration of vapour molecules in the chamber. The current can then be amplified for a signal readout. To be detected, the ionisation energy of the molecules being monitored cannot exceed the energy of the incident UV light. Therefore, molecules of clean air will not be detected. Likewise, volatile organic compounds with high ionisation energy — such as methane — will not be recognised by the PID. Conversely, if the energy is required to ionise a volatile of interest is relatively low, the PID will generally show a relatively large response to that volatile [1], [2].

1. Vapour Sensing System for Transistor Biosensing

The photoionisation detector used in this work had a lamp energy of 10.6 eV, with a quoted response time of less than 2 seconds. Photoionisation detectors are designed to sensitively detect within a particular concentration range. PID sensors can become less sensitive after being exposed to very high concentrations of volatile gas. They can also become less sensitive if exposed to high levels of humidity or volatile substances known to contaminate the PID window, which are not used in this thesis. The typical sensitivity range of a PID can be stated in terms of the sensor response to isobutylene gas, which is typically used to calibrate PID sensors. The sensitivity of the the PID sensor used here was 10 ppb – 200 ppm. Calibration with a reference gas ensures the detector reads the true concentration of volatiles being detected, multiplied by some previously-documented factor called a “response factor”. However, these response factors can vary based on the design of the PID and various environmental factors [1], [2].

In this work, the PID was operated without end-user calibration. PID measurements were used to confirm the evolution of vapour presence in the chamber over time. It should be expected that sensor sensitivity will exhibit span drift over days or weeks, depending on changes in the local environment, and therefore measurements should not be treated as absolute measurements that correspond to a true concentration reading. A sampling rate of 1 s was used for all measurements. When sampling vapour concentration, baseline measurements of nitrogen flow through the PID were used as the zero concentration reference point.

The vapour of interest can be delivered to the PID either through diffusion or by means of a low-power pump. A micro diaphragm pump (Xavitech) was selected to pump the vapour from the chamber into the PID detector. A pump with a low maximum flow rate was selected since the PID requires a inlet flow of less than 300 sccm. As the pump is controlled using a unlabelled dial, a flowmeter was used to independently measure the flow rate through the micropump into the PID.

1.2.3. Control System

The vapour delivery system was controlled and monitored from a laptop connected to a National Instruments USB-6009 multifunction data acquisition input/ output module (DAQ). This USB-6009 DAQ connected to the mass flow controllers and relative humidity and temperature indicator (Telaire) via a custom-designed circuit board manufactured by PCBway. The outputs and inputs of the USB-6009 DAQ were set using custom LabView software. These electronic and software components of the vapour delivery control system are described in more detail below. The photoionisation detector (Ametek Mocon) was controlled from the same laptop with its own prepackaged software (VOC-TRAQ II).

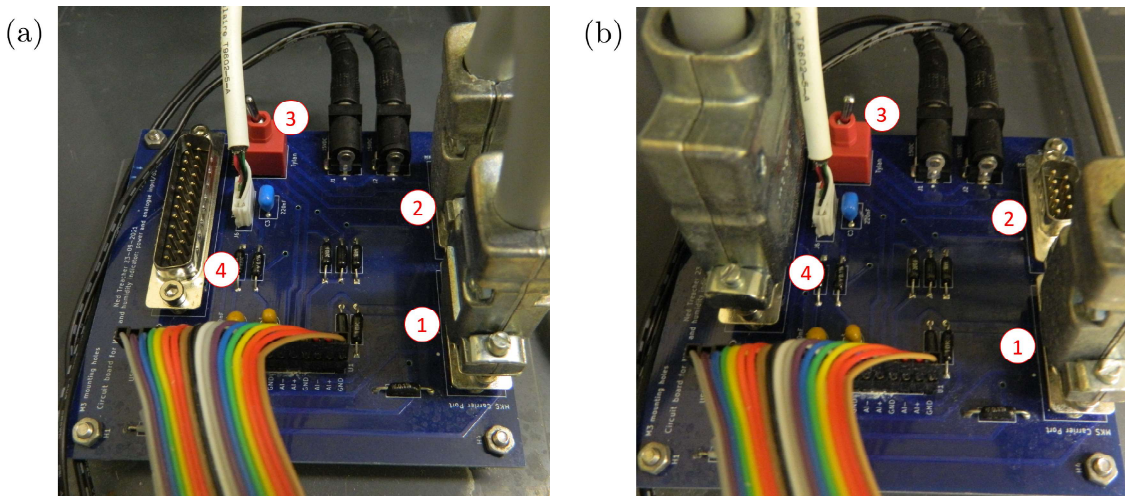


Figure 1.4.: Images of the vapour delivery control system circuit board, where (a) shows the low-flow configuration and (b) shows the high-flow configuration. Components are labelled as follows: (1) 9-pin carrier line port, (2) 9-pin dilution line port, (3) dilution port switch (determines which dilution line port is active), (4) 25-pin dilution line port. In (a), the 500 sccm full-scale MFC is connected at the 25-pin dilution line port, the 200 sccm full-scale MFC is connected at the 9-pin carrier line port and the red dilution port switch is towards “Tylan” (to the right). In (b), the 200 sccm full-scale MFC is connected at the 9-pin dilution line port, the 20 sccm full-scale MFC is connected at the 9-pin carrier line port and the red dilution port switch is towards “MKS” (to the left).

1. Vapour Sensing System for Transistor Biosensing

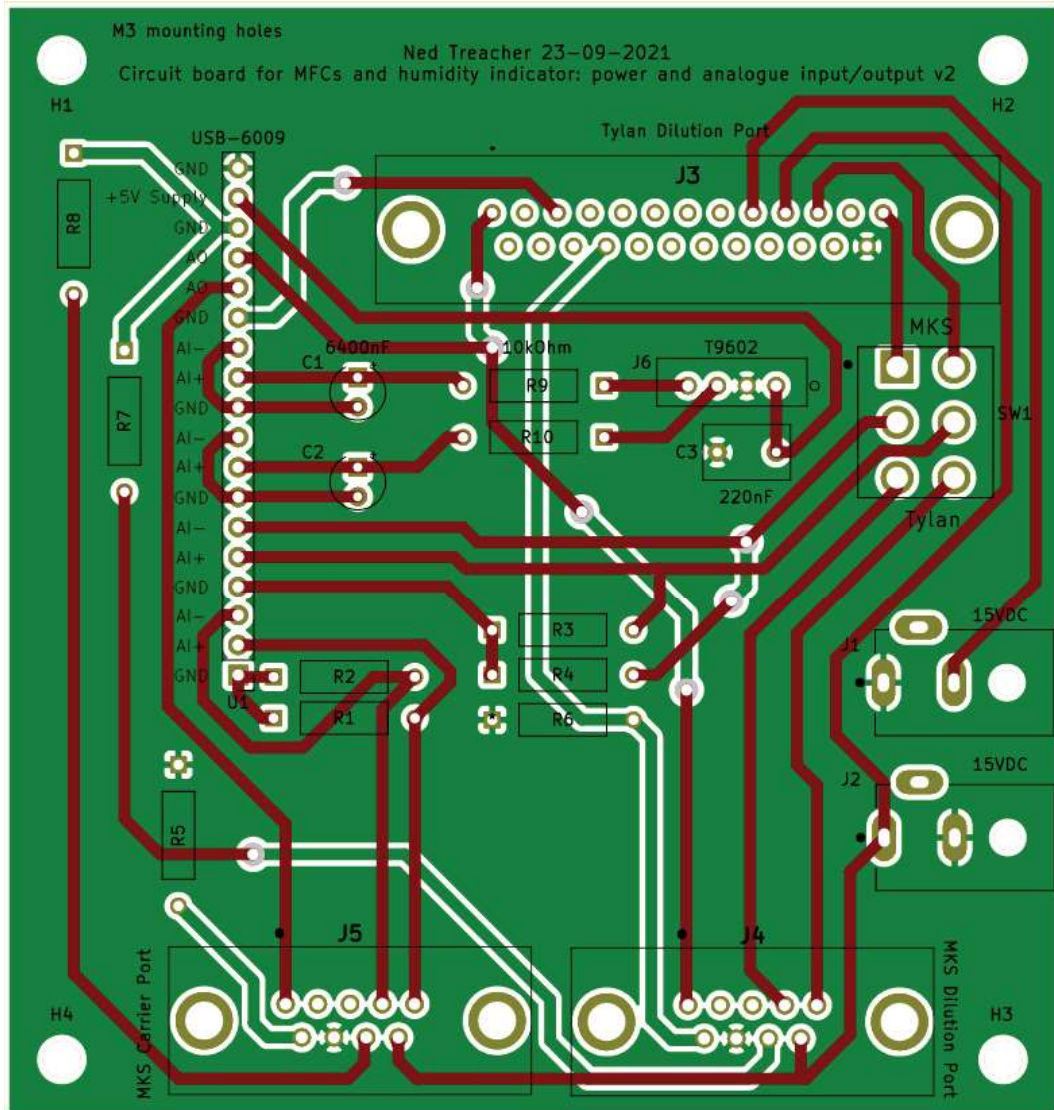


Figure 1.5.: Circuit board schematic for controlling and monitoring both the mass flow controllers and the relative humidity and temperature sensor. The relative humidity and temperature sensor is connected to the circuit board via the T9602 footprint. The mass flow controllers connect to the board in two configurations. The first (“high-flow”) configuration has the Tylan dilution and MKS carrier ports connected, with switch SW1 in the Tylan direction. The second (“low-flow”) configuration has both MKS ports connected, with switch SW1 connected in the MKS direction. Resistors R1-R6 are all 10 kOhm, while R7-R8 are both 0 Ohm. The circuit board was designed using the KiCad Layout Editor.

Electronics

The control circuit board used to connect the mass flow controllers and relative humidity and temperature indicator to the NI USB-6009 is shown in Figure 1.4. Only one mass flow controller can be set to provide flow to a specific line, and so only two mass flow controllers can be operational simultaneously during testing with the vapour delivery system. The control circuit board allows the user to set which two mass flow controllers are to be used during a specific test run. Figure 1.4 (a) shows the “high-flow” configuration, where the 500 sccm full-scale MFC is connected to the dilution line and the 200 sccm full-scale MFC is connected to the carrier line. Figure 1.4 (b) shows the “low-flow” configuration, where the 200 sccm full-scale MFC is connected to the dilution line and the 20 sccm full-scale MFC is connected to the carrier line. The design for the circuit board is shown in Figure 1.5, showing the pinout to the USB-6009 and the various components used to connect the MFCs, relative humidity indicator, and the power supply for the MFCs.

Software

Two LabView Virtual Instruments (VIs) were adapted from pre-existing VIs for operating the mass flow controllers and monitoring vapour flow into the device chamber, as well as monitoring temperature and humidity in the vapour delivery system’s manifold. These VIs were named “vapour-sensor-basic.vi” and “temp-and-humidity-basic.vi”. A third VI was developed in parallel which combined the first two Virtual Instruments and allowed the user to set a sequence of values for the output flow from the mass flow controllers before an experimental run. This VI was named “vapour-sensor-sequence-timestamped.vi”. Flow rate, relative humidity and temperature data were then saved as .lvm files. The LabView VIs described here are available on request.

1.3. Design

1.3.1. Initial Design

The initial design of the vapour delivery system, as shown in Figure 1.6, was relatively simple. No reference sensors were included in the setup, and only one channel could be characterised without opening the chamber and changing the position of the device. However, as constructed it worked well as a self-contained system, which was able to deliver vapour to a device channel while measuring current across the channel. The original system is shown in Figure 1.7, and the circuit board used to control it is shown in @fig-original-pcb. A 500 sccm full-range MFC (Tylan) was placed on the dilution line, and a 200 sccm full-range MFC (Tylan) was placed on the carrier line. A glass container for analyte was present on the carrier line, with a vapour trap upstream to collect any

1. Vapour Sensing System for Transistor Biosensing

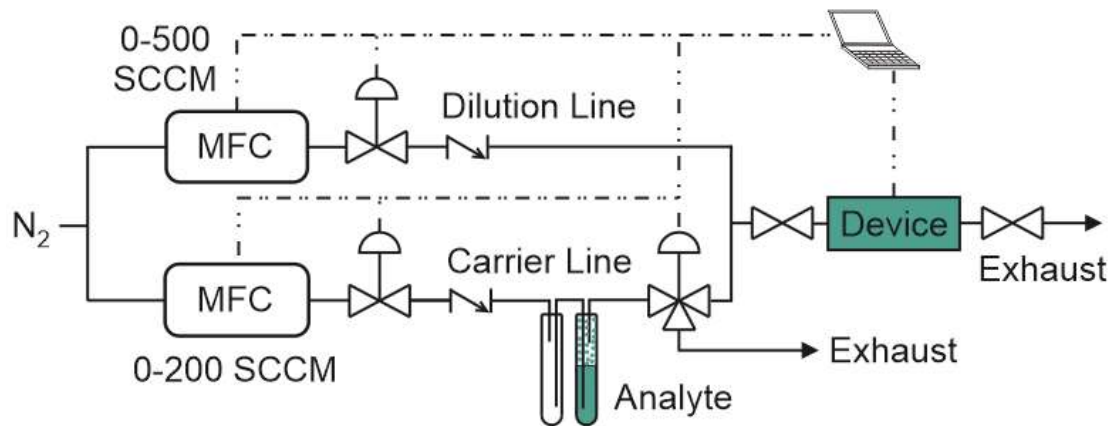


Figure 1.6.: P&ID of the original vapour delivery system

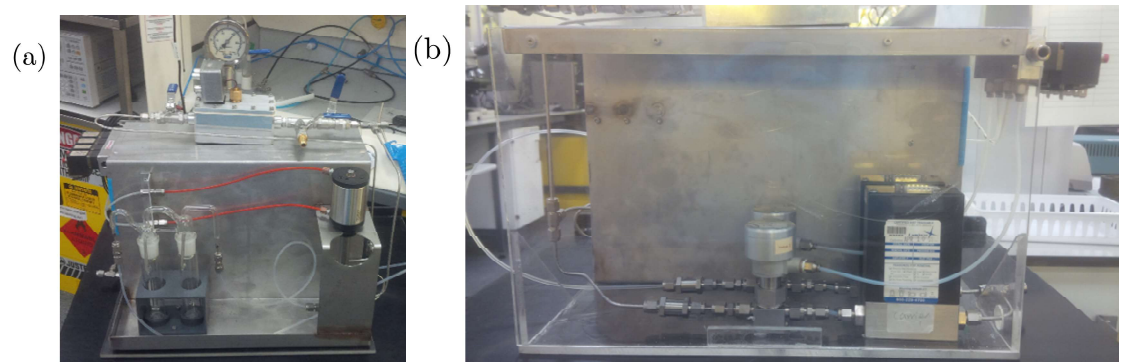


Figure 1.7.: The original vapour delivery system setup, where (a) shows the front of the system, including the device chamber, analyte bottles and four-way valve, and (b) shows the back of the system, including the mass flow controllers and solenoid valves.

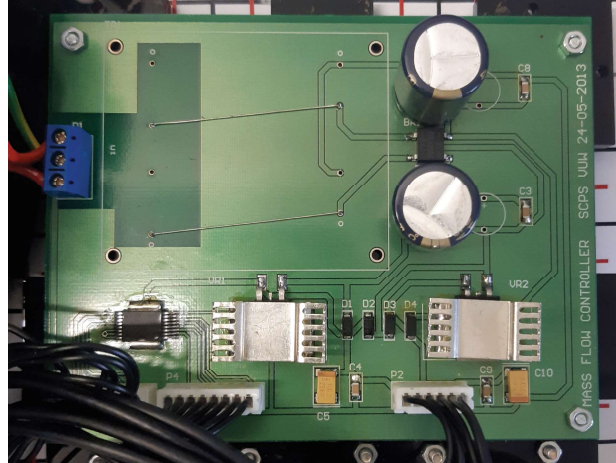


Figure 1.8.: The control circuit board for the original vapour delivery system.

backflow. The vapour trap was removed in later iterations due to the presence of a check valve to prevent backflow. The device chamber and mass flow controllers were connected to a laptop and an Agilent 4156C semiconductor parameter analyser and controlled using LabView.

1.3.2. Stage I Design

The first stage of the vapour delivery system redesign, as shown in Figure 1.9, was implemented in Nov 2021. This system introduced the ability to use a 20 sccm full-range MFC (MKS Instruments) for carrier line flow and a 200 sccm full-range MFC (MKS Instruments) for either carrier or dilution line flow, to give better control when using low flow rates. The reference sensors were also implemented, with each sensor connected in parallel to the chamber exhaust. Through testing the system with ethanol and acetone as analytes, the following issues with this implementation of the setup were identified:

- With the system connected to the lab supply of nitrogen, pressure changes in the line due to nitrogen use elsewhere in the lab impacted the pressure at the MFCs and the flow through the lines.
- The pressure indicator used for the device chamber had a much wider range than the pressure reached before nitrogen began to leak out of the PVC tubing; this meant pressure changes in the chamber, resulting from closing the exit valves while nitrogen flow entered the chamber, did not register on the indicator.
- The PID responded unexpectedly slowly to changes in vapour concentration in the chamber. For example, after acetone or ethanol vapour had been run through

1. Vapour Sensing System for Transistor Biosensing

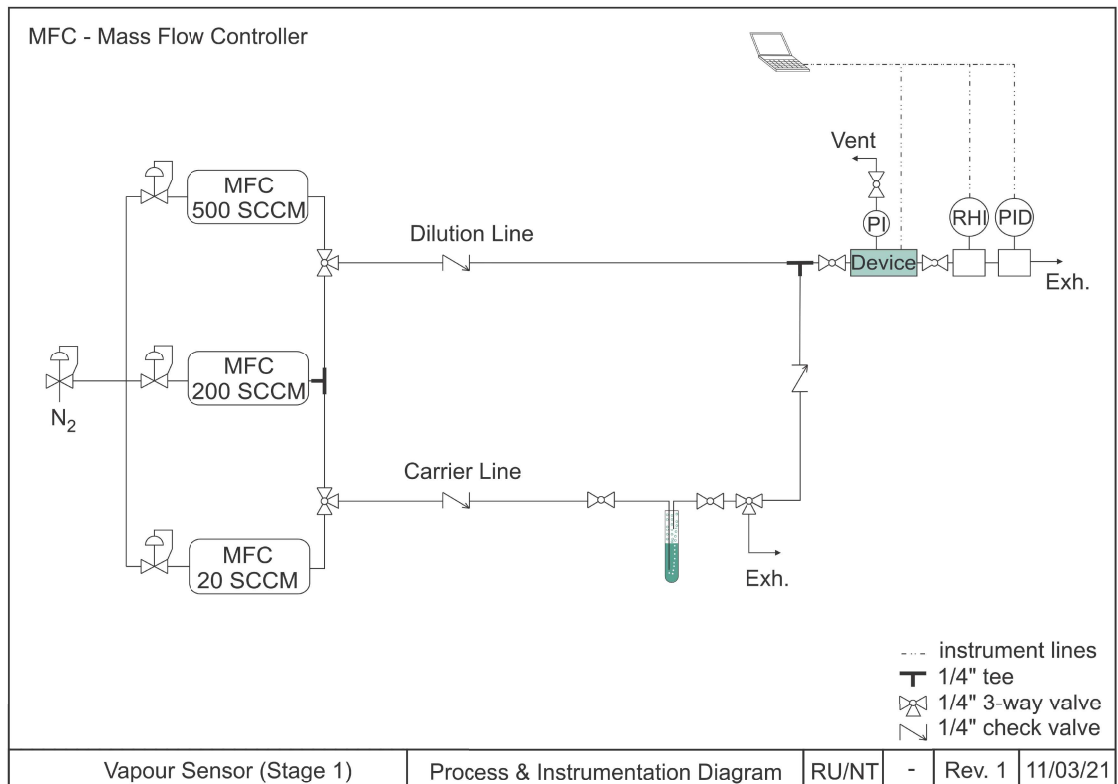


Figure 1.9.: P&ID of the Stage I vapour delivery system.

1.3. Design

the chamber, running clean nitrogen through the system for 3 hours was required before the PID returned to a constant baseline reading.

- There was no way to ensure the device chamber was free of analyte vapour before an experimental run aside from running nitrogen through the dilution line. After prolonged use, condensed analyte was sometimes visible in the PVC lines of the delivery system.

These issues, along with various minor structural and design issues, were addressed in the second-stage implementation of the system.

1.3.3. Stage II Design

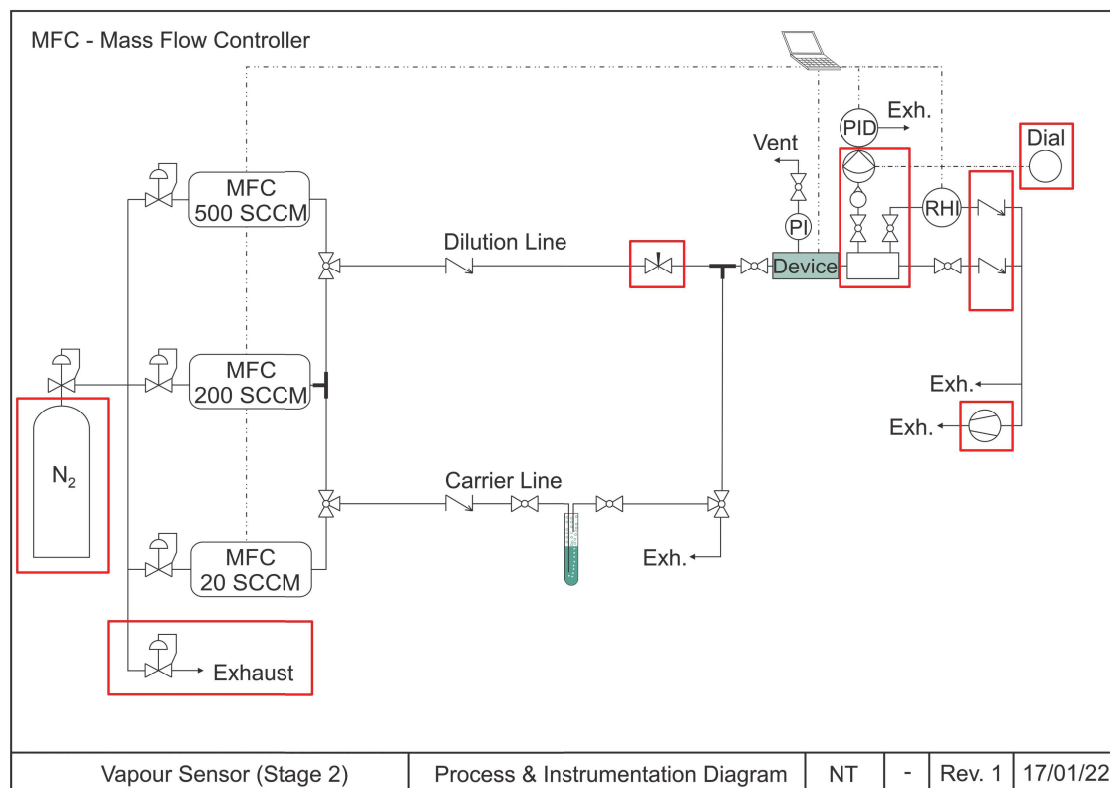


Figure 1.10.: Process & instrumentation diagram (P&ID) of the second-stage design for the vapour delivery system. Red outlines indicate additions introduced to the system subsequent to the first stage design.

Figure 1.10 gives an overview of the second-stage design for the vapour delivery system setup. This stage of the redesign was implemented between Jan and May 2022. Changes from the first stage included:

1. Vapour Sensing System for Transistor Biosensing

- The addition of a N₂ cylinder (152D size) as the source of nitrogen for the system to replace the lab supply.
- A pressure indicator with a lower pressure range was used, which could register pressure changes within the device chamber.
- A chamber manifold was placed before the exhaust with outlets into the PID and RHI.
- A micro diaphragm pump was introduced between the manifold and PID to supply the PID with vapour from the chamber, and a flowmeter was placed before the pump to measure the flow rate out of the chamber to the PID. The PID was then seen to respond quickly to system changes (discussed further in Section 1.4).
- A piece of PVC tubing was placed at the PID outlet to limit air from the fumehood entering the PID when the micropump was off.
- Valves were placed before all system components so that the device chamber and post-analyte bottle carrier line could be evacuated with a roughing pump without potentially affecting components.
- Check valves were placed at the exhaust to prevent backflow from the roughing pump into the delivery system.

These changes largely addressed the issues identified in Section 1.3.2.

1.4. Calibration and Measurements of Vapour Flow

1.4.1. Chamber Flow Calibration

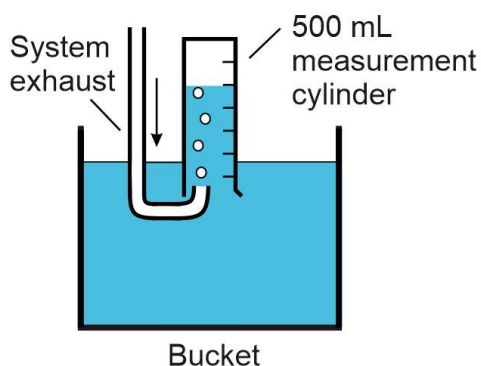


Figure 1.11.: Setup for calibration of mass flow controllers using the water displacement method.

1.4. Calibration and Measurements of Vapour Flow

A water displacement test was carried out to determine the relationship between the flow rate measured by the mass flow controllers and the actual flow rate passing through the chamber. All valves were set so that both the dilution and carrier lines followed a single path. Both these paths went through the device chamber and out through the system exhaust. An empty analyte bottle was placed on the carrier line. The system exhaust was placed into a bucket filled with tap water, with the outlet sitting beneath an upturned 500 mL measurement cylinder, as pictured in Figure 1.11. The cylinder was used to measure the volume of displaced water over time, which is equivalent to the rate of change of nitrogen volume entering the cylinder from the exhaust. Measurements were taken from the bottom of the menicus of the water in the cylinder. As leaks in the manifold and exhaust line were not detected when leak testing with bubble solution, it can be safely assumed that the rate at which nitrogen exits the exhaust is equivalent to the nitrogen flow rate through the device chamber.

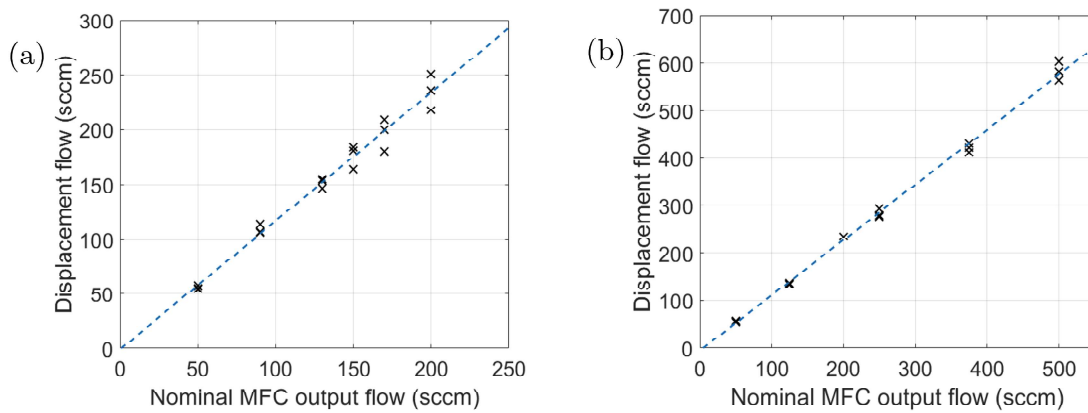


Figure 1.12.: The nominal flow rate as measured by the mass flow controller compared to the actual flow rate measured using water displacement testing, shown for the 200 sccm full-scale mas flow controller placed through the carrier line in (a), and for the 500 sccm full-scale mass flow controller placed through the dilution line in (b). Three water displacement tests were performed for each constant flow rate. A strong linear relationship between nominal and actual flows was identified using least-squares methods, shown by a blue dotted trendline. The fit shown in (a) had an R-squared value of 0.98, while the fit in (b) had an R-squared value of 0.997.

The time taken to displace 50 mL of water was measured three times for a series of constant flow rates, both for the 200 sccm MFC (MKS) on the carrier line and the 500 sccm MFC (Tylan) on the dilution line. The displacement flow rate corresponding to each measurement could then be found by dividing volume by time. These measurements, of displacement flow relative to nominal flow through the MFC, are shown in Figure 1.12. The increased uncertainty for higher flow measurements is predominantly due to the increased difficulty of precise measurement of these more rapid flows using the water

1. Vapour Sensing System for Transistor Biosensing

displacement tests. However, increased instability of flow from the MFCs at higher flow rates may also contribute to this uncertainty.

The flow through the chamber was offset from the nominal flow reading from the mass flow controllers; a strong linear relationship was found to exist between the two measurements. A linear least-squares fit was performed, where coefficients a_1 and a_2 were found for the linear relationship $D = a_1d + a_2$, where d is nominal flow from the MFC and D is measured displacement flow. A 95% confidence interval for each fit was also obtained. For the 200 sccm MFC flow through the carrier line, values of $a_1 = 1.18 \pm 0.09$ and $a_2 = -1 \pm 13$ were obtained, while for the 500 sccm MFC flow through the dilution line, values of $a_1 = 1.16 \pm 0.04$ and $a_2 = -5 \pm 10$ were obtained.

It appears that the offset between the measured displacement flow and nominal output flow is not due to leaks in the system, since the offset indicates measured flow exceeds the nominal flow. Instead, the offset appears to be a systematic error introduced by the electronics or software used to record the output flow from the MFCs. The identical offset between measured and nominal flow observed for each MFC, even when placed on different lines to the chamber, further strengthens the likelihood of the offset being due to the control side of the system. Furthermore, as both the carrier and dilution MFCs show readings with the same offset multiplier within a 95% confidence interval, the same offset should apply to a mixture of flows on each line. For example, a 200 sccm nominal flow through the dilution line from the 500 sccm full-scale MFC should have a roughly identical actual flow rate to a 50 sccm nominal flow through the dilution line and a 150 sccm flow through the carrier line. In this work, tests performed with the vapour delivery system have flow rate stated in terms of their nominal value. However, the reader should keep in mind the $1.16 - 1.18 \times$ offset between the nominal and actual chamber flow.

The time taken to displace a fixed water volume was also measured three times for a series of constant flow rates through the flowmeter from the chamber to exhaust. A least-squares linear relationship was obtained between flowmeter readings and actual displacement, as shown in Figure 1.13. Expressing the relationship as $D = b_1f + b_2$, where f is the flowmeter reading and D is measured displacement flow, values of $b_1 = 0.85 \pm 0.2$ and $b_2 = -18 \pm 26$ were obtained. A 200 sccm flow rate through the dilution line from the Tylan MFC, corresponding to a ~ 230 sccm actual flow rate through the chamber, would therefore be measured as a ~ 150 sccm flow rate by the flowmeter. The R-squared value for the fit was 0.87.

Note that the flow reading by the flowmeter became more unstable for flows above 150 sccm and below 130 sccm, leading to reduced repeatability and increased uncertainty of measurements taken for these higher and lower flow rates. To understand the reason for this instability, flow through the chamber was placed directly through the flowmeter without the micropump present. Stable readings could then be achieved, indicating that the flow rate instability at higher or lower flows results from limitations of the micropump used for vapour delivery. As the flow rate from the micropump was relatively stable between 130 – 150 sccm, a micropump flow measured as 150 sccm on the flowmeter

1.4. Calibration and Measurements of Vapour Flow

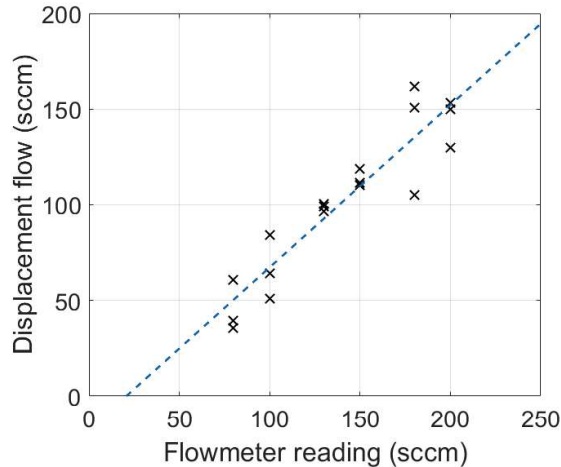


Figure 1.13.: Comparison of flowmeter readings with flow measurements from water displacement testing. Three water displacement tests were performed for each constant flow rate. A linear least-squares fit is shown by the blue dotted line, with an R-squared value of 0.87.

was generally used when measuring vapour flow through the delivery system to the photoionisation detector. From Figure 1.13 it can be seen that this corresponds to an actual flow of ~ 110 sccm, about 50% of the actual flow passing through the chamber when the total output flow of the mass flow controllers is set at 200 sccm.

1.4.2. Sensor Responses to Vapour Flow

Once the rate of flow through the device chamber had been calibrated, the next step was to verify the correct operation of the reference sensors used in the system. Various flow rates in and out of the chamber were used to calibrate and verify the reference sensors. These flows in and out of the chamber are labelled on the simplified schematic in Figure 1.14.

Relative Humidity Indicator

To test the relative humidity indicator (RHI), all valves out of the chamber were sealed except for the valve for the relative humidity indicator chamber. This meant all flow coming out of the system would pass through the relative humidity indicator chamber ($P = 0$ sccm and exhaust goes to RHI in Figure 1.14). Continuous nitrogen flow was then placed through the chamber until relative humidity dropped to about 20%. 10 mL of deionised water was placed into the analyte bottle. A series of different flow rates through each line was sent to the chamber, with the sequence of flow rates shown in Table 1.1 (t = time, C = carrier line flow rate, D = dilution line flow rate). Note that

1. Vapour Sensing System for Transistor Biosensing

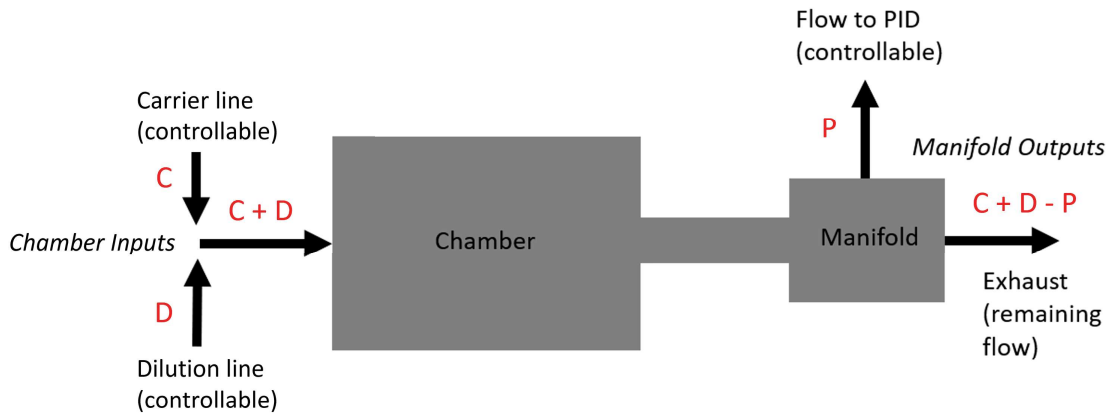


Figure 1.14.: Simplified schematic showing the flow into and out of the device chamber and manifold of the delivery system. The input flows from the carrier and dilution line are represented by C and D, and the output flow through the PID is represented by P. The exhaust can either flow past the relative humidity indicator or straight to the fumehood. This diagram assumes that flow through leaks in the chamber and manifold is low enough to be considered negligible, which was confirmed by leak testing with bubble solution.

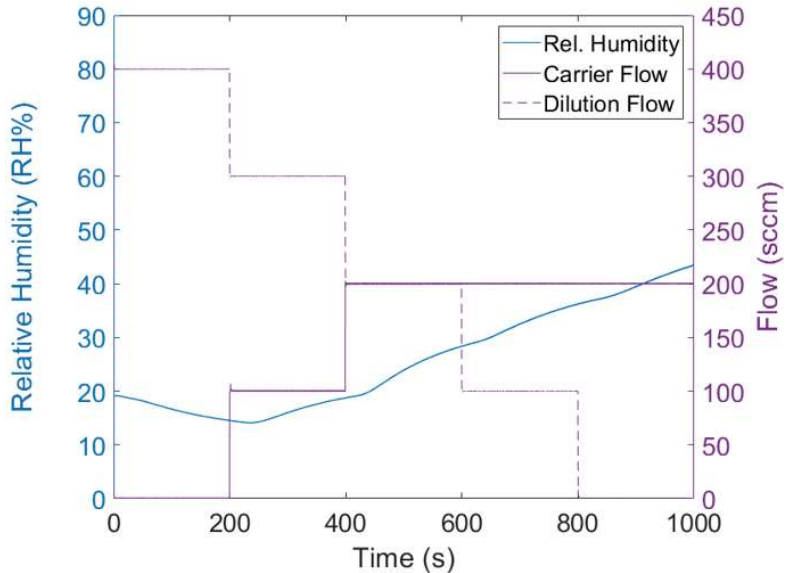


Figure 1.15.: Relative humidity readouts from the relative humidity indicator juxtaposed with flow rates from the dilution line and carrier lines of the vapour system, with 10 mL deionised water in the carrier line analyte bottle.

1.4. Calibration and Measurements of Vapour Flow

between 230 s and 630 s, the total flow rate remains the same, but the ratio of dilution to carrier flow differs.

Figure 1.15 shows flow purely from the dilution line decreases humidity as measured by the Telaire sensor, while flow from the analyte bottle containing deionised water increases humidity, as expected. It also shows that in regular 200 s intervals, an uptick in the increase of relative humidity occurs, which then begins to flatten out. Each gradient uptick occurs about 50 s after a corresponding increase in flow through the carrier line. It therefore appears that each interval corresponds to an increase of water vapour flow, where 50 s is the time taken for the increased concentration of water vapour to first reach the relative humidity indicator.

Table 1.1.: Flow sequence for testing relative humidity indicator.

t (s)	C (sccm)	D (sccm)
200	0	400
200	100	300
200	200	200
200	200	100
200	200	0

Over the full 800 s of carrier line flow, relative humidity increases from a minimum of $14.0 \pm 2.0\%$ to a maximum of $43.6 \pm 2.0\%$. The temperature in the chamber remained between $21.0 \pm 0.5^\circ\text{C}$ and $22.0 \pm 0.5^\circ\text{C}$ over the entire measurement period. Combining equations Equation 1.1 and Equation 1.2 from Section 1.2.2, we find that the absolute humidity in the chamber reaches a low of $2.6 \pm 0.4 \text{ gm}^{-3}$ at 238.1 s, 38.1 s after the initial onset of carrier flow, and a high of $8.4 \pm 0.5 \text{ gm}^{-3}$ at 998.8 s, after 798.8 s of carrier flow through the chamber. The clear response of the Telaire RHI to water vapour flow through the carrier line confirms that this sensor is working as expected.

Photoionisation Detector with Continuous Vapour Flow

To test the photoionisation detector, the device chamber and carrier line were first purged of vapour through the exhaust using a roughing pump, with the PID valve closed to protect it from the pump. The PID valve was then opened, the micropump was set to 150 sccm as read by the flowmeter. During testing with the PID, the total flow into the chamber was set at 200 sccm as read by the Tylan mass flow controllers. The calibration curves in Section 1.4.1 show that the actual flow $C + D$ was then therefore approximately the same as the actual flow rate into the PID, P . A flow of 200 sccm nitrogen was placed through the dilution line to the chamber for 10 minutes until successive concentration readings from the PID were either approximately constant, or until baseline drift was small enough to be considered negligible. These measurements were then used as the

1. Vapour Sensing System for Transistor Biosensing

baseline (0 ppm) for subsequent measurements. 5 mL of the volatile organic compound ethyl hexanoate (EtHex) was placed into the analyte bottle. A flow of 150 sccm was then sent through the carrier line and 50 sccm through the dilution line for 600 s. The same procedure was performed on two separate dates spaced three days apart (23 Feb and 26 Feb) to check that the measured PID response to ethyl hexanoate vapour pumped out of the manifold was repeatable.

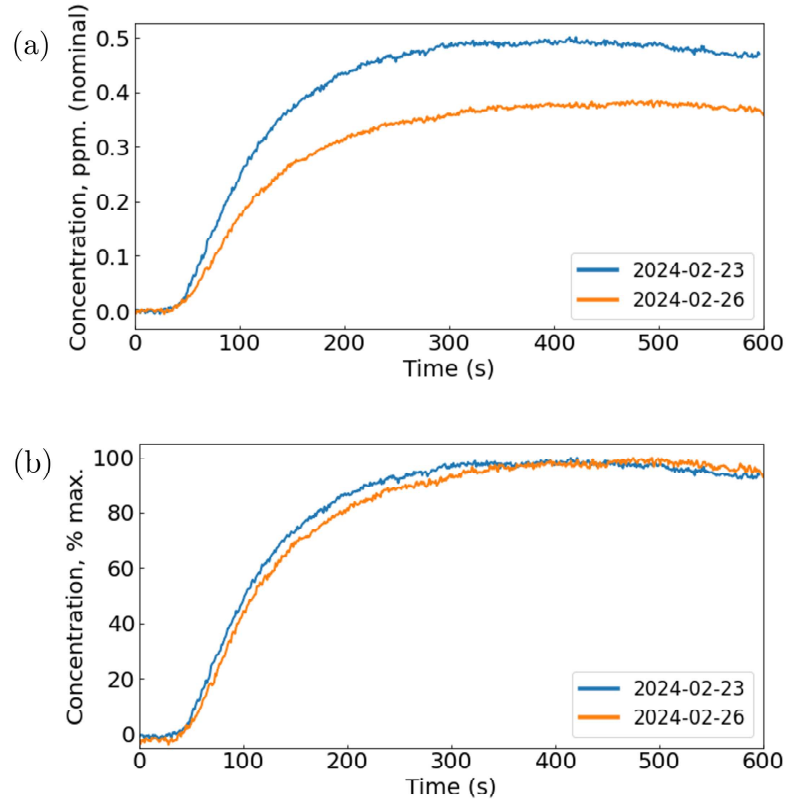


Figure 1.16.: The response of the photoionisation detector to ethyl hexanoate vapour over 600 s of exposure is shown relative to the 200 sccm nitrogen flow baseline in (a), and normalised with respect to the maximum reading in (b).

The responses from each date are shown in Figure 1.16. In Figure 1.16 (a), the response corresponding to each measurement date is shown unnormalised, with the parts per million concentration shown relative to the nitrogen baseline as recorded by the PID. Both measurements show little to no response to vapour for approximately 50 s, which seems to be the time taken for vapour to first reach the PID. Over the next 100s, there is a rapid increase in vapour concentration detected, which then settles to a constant concentration at about 300 s. This appears to be the maximum concentration of EtHex vapour that can be contained by the chamber in this configuration. There is approximately a

1.4. Calibration and Measurements of Vapour Flow

200 parts per billion difference in maximum concentration between the measurement on each date.

However, this is not unexpected. As discussed in Section 1.2.2, the PID is being run uncalibrated, and some drift of the sensitivity of the sensor due to environmental changes is highly likely. To check that the PID records the same evolution of vapour flow with time, regardless of its sensitivity, the measurements from both dates were then normalised with respect to the maximum concentration reading. Figure 1.16 (b) shows that once normalised, the rate of change in concentration with time is almost identical between the two measurement sets. This test verifies that the evolution of vapour concentration of the device chamber can be repeatably measured using the PID in the vapour delivery system.

Photoionisation Detector with Vapour Flow Intervals

A further series of tests were performed to verify whether it was possible to compare different concentrations of vapour in the chamber using the PID. All testing was performed on the same day to minimise sensitivity drift. For each test, the system was purged of vapour and the total dilution flow into the chamber was set at 200 sccm as read by the Tylan mass flow controller. Flow out of the chamber to the PID was set at 100 sccm as read by the micropump flowmeter, and the almost-constant nitrogen baseline after 10 minutes was set as the PID zero point. 5 mL of the volatile organic compound ethyl hexanoate (EtHex) was placed into the analyte bottle. During each test, 200 sccm was continuously flowed through the dilution line, except during three evenly spaced intervals of equal length. During these intervals, 150 sccm flow was placed through the carrier line and 50 sccm flow placed through the dilution line. In each test, the input interval time was varied to examine its effect on maximum vapour concentration recorded by the PID. As it took longer for the PID to return to a constant baseline with increased input intervals, when the input interval was increased, the spacing between intervals was also increased.

The results of three tests, with input intervals of 50 s, 100 s and 200 s, are shown in Figure 1.17. Each interval of carrier flow corresponds to a rapid increase in concentration, which reaches a peak, then decreases. The maximum concentration reached for each interval is shown above the corresponding peak. Note that the maximum concentration label does not correspond to the difference between the original baseline and the maximum concentration of each peak. Instead, it corresponds to the difference between the concentration measurement at a set time before the onset of carrier flow and the maximum concentration reached. For each test, this set time is 5% of the spacing time used, 50 s, 150 s and 300 s respectively. This approach was taken to account for what appears to be drift from the original 0 ppm baseline. This variable baseline drift was particularly significant for the 100 s interval measurements, where concentration measurements settled to a new baseline of ~ 0.05 ppm after the third peak.

1. Vapour Sensing System for Transistor Biosensing

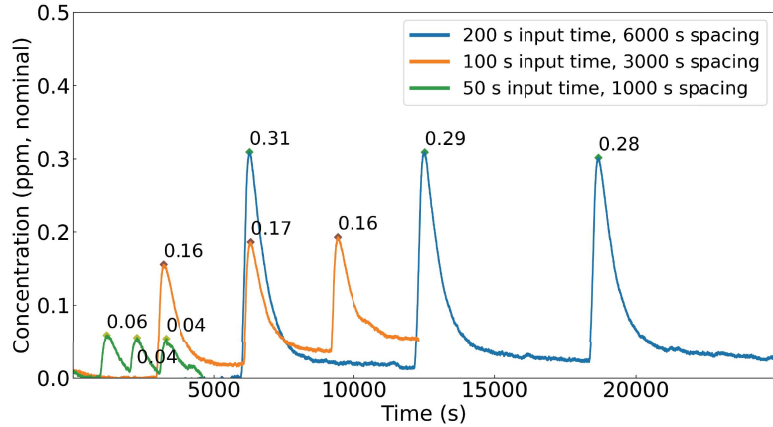


Figure 1.17.: The response of the photoionisation detector to 3 evenly-spaced intervals of ethyl hexanoate vapour entering the device chamber, relative to a 200 sccm nitrogen flow baseline. Input intervals were either either 50 s, 100 s or 200 s in length. During each input interval, 150 sccm carrier flow and 50 sccm dilution flow was placed through the chamber.

The values of three concentration maxima in each test are highly consistent, with only a ± 0.02 ppm margin of error. This experiment demonstrates that if tests using the PID are performed during the same day, placing the same vapour flow into the PID for the same interval of time in each test, it is possible to measure the same maximum concentration with the PID. It furthermore indicates that the placing the same amount of vapour flow into the chamber for a set amount of time leads to a reproducible concentration of vapour building up within the chamber.

1.5. Summary

A custom vapour delivery system was made suitable for field-effect biosensor work through ensuring a range of flows could be delivered through the system and that reference sensors were available for corroboration with the readings on the field-effect biosensors. Two new mass flow controllers with different maximum flow rates and two reference sensors, a relative humidity and temperature sensor and photoionisation detector, were introduced to the system in a two-stage design process. A new electronic control system and LabView software were designed and constructed for the altered delivery system. The nitrogen flow through the system was then calibrated using water displacement testing, and it was verified that the reference sensors both worked as expected.

A. Vapour System Hardware

Table A.1.: Major components used in construction of the vapour delivery system described in this thesis.

Description	Part No.	Manufacturer
Mass flow controller, 20 sccm full scale	GE50A013201SBV020	MKS Instruments
Mass flow controller, 200 sccm full scale	GE50A013202SBV020	MKS Instruments
Mass flow controller, 500 sccm full scale	FC-2901V	Tylan
Analogue flowmeter, 240 sccm max. flow	116261-30	Dwyer
Micro diaphragm pump	P200-B3C5V-35000	Xavitech
Analogue flow controller, for micro diaphragm pump	X3000450	Xavitech
10 mL Schott bottle	218010802	Duran
PTFE connection cap system	Z742273	Duran
Baseline VOC-TRAQ flow cell, red	043-951	Mocon
Humidity and temperature sensor	T9602	Telaire
Enclosure, for humidity and temperature sensor	MC001189	Multicomp Pro

B. Python Code for Data Analysis

B.1. Code Repository

The code used for general analysis of field-effect transistor devices in this thesis was written with Python 3.8.8. Contributors to the code used include Erica Cassie, Erica Happe, Marissa Dierkes and Leo Browning. The code is located on GitHub and the research group OneDrive, and is available on request.

B.2. Atomic Force Microscope Histogram Analysis

The purpose of this code is to analyse atomic force microscope (AFM) images of carbon nanotube networks in .xyz format taken using an atomic force microscope and processed in Gwyddion (see [?@sec-afm-characterisation](#)). It was originally designed by Erica Happe in Matlab, and adapted by Marissa Dierkes and myself for use in Python. The code imports the .xyz data and sorts it into bins 0.15 nm in size for processing. To perform skew-normal distribution fits, both *scipy.optimize.curve_fit* and *scipy.stats.skewnorm* modules are used in this code.

B.3. Raman Spectroscopy Analysis

The purpose of this code is to analyse a series of Raman spectra taken at different points on a single film (see [?@sec-raman-characterisation](#)). Data is imported in a series of tab-delimited text files, with the low wavenumber spectrum ($100\text{ cm}^{-1} - 650\text{ cm}^{-1}$) and high wavenumber spectrum ($1300\text{ cm}^{-1} - 1650\text{ cm}^{-1}$) imported in separate datafiles for each scan location.

B.4. Field-Effect Transistor Analysis

The purpose of this code is to analyse electrical measurements taken of field-effect transistor (FET) devices. Electrical measurements were either taken from the Keysight 4156C Semiconductor Parameter Analyser, National Instruments NI-PXIe or Keysight B1500A Semiconductor Device Analyser as discussed in [?@sec-electrical-characterisation](#);

B. Python Code for Data Analysis

the code is able to analyse data in .csv format taken from all three measurement setups. The main Python file in the code base consists of three related but independent modules: the first analyses and plots sensing data from the FET devices, the second analyses and plots transfer characteristics from channels across a device, and the third compares individual channel characteristics before and after a modification or after each of several modifications. The code base also features a separate config file and style sheet which govern the behaviour of the main code. The code base was designed collaboratively by myself and Erica Cassie over GitHub using the Sourcetree Git GUI.

Bibliography

- [1] “piD-TECH® eVx User Manual 143-175 Rev 1.0”. URL: <https://www.ametekmocon.com/products/oemphotoionization/pidtechevxphotoionizationdetector>.
- [2] *Technical Application Articles - Ion Science UK*. URL: <https://ionscience.com/en/gas-and-leak-detectors/customer-support/support-documents/technical-application-articles/> (visited on 2024-02-27).
- [3] Amphenol Advanced Sensors. *Telaire T9602 Humidity and Temperature Sensor*. URL: <https://www.amphenol-sensors.com/en/telaire/humidity/527-humidity-sensors/3224-t9602> (visited on 2024-02-26).
- [4] *The Capacitive Humidity Sensor*. URL: https://www.rotronic.com/en/humidity-measurement-feuchtemessung-mesure_de_1_humidite/capacitive-sensors-technical-notes-mr (visited on 2024-02-26).
- [5] *Make Your Job Easier with Humidity Conversion Formulas / Vaisala*. URL: <https://www.vaisala.com/en/lp/make-your-job-easier-humidity-conversion-formulas> (visited on 2024-02-26).